Advances in Water Resources **15** (1992) 275–287

A three-dimensional numerical model for water flow and transport of chemically reactive solute through porous media under variably saturated conditions

Rajesh Srivastava & T.-C. Jim Yeh

Department of Hydrology and Water Resources, University of Arizona, Tucson, Arizona 85721, USA

A three-dimensional numerical model is developed for the simulation of water flow and chemical transport through variably saturated porous media. The nonlinear flow equation is solved using the Galerkin finite element technique with the Picard iteration scheme and a continuous velocity field is obtained by separate application of the Galerkin technique to the flux equation. A two-site adsorption–desorption model with a first-order loss term is used to describe the chemical behavior of the reactive solute. The advective part of the transport equation is solved with one-step backward particle tracking while the dispersive part is solved by the regular Galerkin finite element technique. Preconditioned conjugate-gradient-like method is used for the iterative solution of the systems of linear simultaneous equations to save on computer memory and execution time. The model is applied to a few situations and the numerical results are compared with observed and analytic values. The model is found to work quite well, even near very sharp fronts.

Key words: variably saturated flow, chemical transport, finite element method, modified method of characteristics.

INTRODUCTION

Until the early 1970s, studies of flow and transport through unsaturated soils were limited to the upper 1 m of the vadose zone and were done primarily with agricultural purposes in mind. Because of the important role of the vadose zone in groundwater pollution problems, in the last 20 years, hydrologists have become increasingly interested in studies involving unsaturated flow and transport problems on scales of meters and tens of meters. At such large scales, the hydrological properties of the geologic media exhibit a large degree of spatial variation. For investigating and predicting contaminant migration in large-scale geologic media, mathematical modeling is generally required. However, analytic solutions to such problems are almost impossible to obtain and numerical modeling becomes the method of choice for analyzing and predicting the movement of contaminants through the subsurface media (Anderson[1]). The mathematical models are generally based on the governing equation for flow under variably saturated conditions (Richards equation) and the classic convection–dispersion equation. One of the difficulties in predicting the movement of contaminants lies in our lack of ability of solving these equations accurately and efficiently for general cases.

The dependence of hydraulic properties of unsaturated media on the pressure or degree of saturation makes the Richards equation nonlinear. The degree of nonlinearity of the equation, in turn, depends on the extent of the nonlinearity in hydraulic properties and pressure relationships of media. For general conditions, numerical methods combined with some iterative schemes are required to obtain the solution to this equation. Since hydraulic properties and pressure relationships of some porous media are highly nonlinear, difficulties in obtaining the convergence of the numerical solution and serious mass balance problems have often been encountered (e.g. Celia *et al.*[5]).

The solution of the convection–dispersion equation requires the knowledge of the velocity distribution throughout the solution domain. Many difficulties exist in calculating the velocity field from the pressure

Advances in Water Resources 0309-1708/93/$06.00

distribution obtained by numerical models. As is customary for finite element flow simulation, the nodal heads are treated as unknowns and are assumed to vary linearly in triangular prism elements and tri-linearly in rectangular prism elements. This results in a constant specific discharge value within each element and a consequent discontinuity in the nodal values of the specific discharge. Such a discontinuous discharge field may lead to undesirable numerical solutions of the convection–dispersion equation (e.g. Goode[12]).

Another difficulty in solving the convection–dispersion equation can be attributed to the change in the nature of the equation from parabolic to almost hyperbolic as the advective transport becomes prominent relative to the dispersive transport (manifested by a large Peclet number). While a parabolic partial differential equation is amenable to the commonly used numerical methods like finite difference or finite elements, numerical solution to a hyperbolic equation generally introduces numerical dispersion and oscillation near the sharp front. This problem can be tackled, to some extent, by a properly chosen grid size and time step at the expense of increased computer time and memory requirement. In three-dimensional problems, however, it may not be feasible to do so due to computer memory and execution time limitations. Various alternative approaches have been suggested in the past to reduce the numerical error near the sharp fronts. These include the implicit diffusive finite difference method,[27] upstream weighted finite element method,[13] method of characteristics,[14] modified method of characteristics,[6] Laplace transform Galerkin technique,[24] and the zoomable hidden mesh approach.[29] The method of characteristics (also called the forward particle tracking) and the modified method of characteristics (backward particle tracking) have been combined successfully by some investigators.[3,18] This scheme has been shown to handle the sharp fronts very well but is computationally intensive.

Most of the schemes described above perform well under saturated flow conditions, but have not been rigorously tested for an unsaturated case. Also, there are very few numerical codes for simulation of three-dimensional flow and transport of reactive chemicals in variably saturated media. In this paper, the authors combine several previously developed ideas and construct an efficient, three-dimensional finite element model, which eliminates the difficulties discussed above. The model was applied to several scenarios where either analytical or observed data are available for verification purposes. In additon, analytical solutions of the velocity field in a two-dimensional unsaturated medium with hypothetical hydraulic properties were derived and used to verify the accuracy of the numerical model. The authors believe the development of the model will enhance our ability of predicting flow and fate and transport of contaminants in the field, where hydraulic and geochemical properties of media are inherently heterogeneous.

GOVERNING EQUATIONS

Equation of flow in variably saturated media

The following equation is taken as the equation governing three-dimensional flow of water in porous media:[2]

$$\frac{\partial}{\partial x_i}\left(K_{ij}\frac{\partial}{\partial x_j}(\psi + x_3)\right) = (C + \beta_s S_s)\frac{\partial \psi}{\partial t} - q_s \quad \text{in } \Omega \tag{1}$$

where x_i are the spatial coordinates ($i = 1, 2, 3$ with x_3 being vertical); K_{ij} is the hydraulic conductivity tensor which is a function of moisture content or pressure under unsaturated conditions; ψ is the pressure head; C is the specific moisture capacity and is defined as $d\theta/d\psi$, where θ is the volumetric moisture content; β_s is the index for saturation and is 0 in the unsaturated zone ($\psi < 0$) and 1 in saturated zone ($\psi \geq 0$); S_s is the specific storage defined as the volume of water released from storage per unit volume of saturated soil due to unit decrease in the pressure head; t is the time; q_s is the source/sink term (positive for source) which represents the volume of water added/removed per unit time to/from a unit volume of soil; and Ω is the solution domain. Einstein's summation convention (over repeated index) has been used in the above equation and throughout this paper.

In this study the saturated hydraulic conductivity and the specific storage are assumed to be functions of space only and are considered independent of time. Also, since in the unsaturated region of the flow the storage is controlled predominantly by the moisture content as compared to the compressibility effects, the index β_s is put equal to 0 in unsaturated zone. In saturated porous media, the specific moisture capacity, C, is 0 and the specific storage is generally expressed by $S_s = \gamma_w(\beta_p + \eta\beta_w)$, where γ_w is the unit weight of water, η is the porosity, and β_p and β_w are the coefficients of compressibility of the porous medium and water, respectively.

Equations for transport and fate of contaminants

The complex process of dispersion, adsorption and decay of chemicals in porous media flow is not very well understood at the present time and various models have been proposed to describe the interaction between solute, pore-water and the solid matrix in a porous medium. These models include a simple linear isotherm equilibrium model,[21] a linear reversible adsorption (one-site) model,[17] a two-site adsorption–desorption

model,[4,23] mobile–immobile zone physical partitioning model,[8,26] mobile–immobile zone with ion-exchange[15] and the two-site model with a first-order loss.[16] It has been shown[19] that although the physical partitioning model with mobile and immobile zones and the two-site chemical partitioning model are completely different concepts, they result in the same mathematical equation. Also, Lassey's[16] model is quite general and encompasses, as special cases, the physical and chemical partitioning models. In this paper, therefore, the two-site model with first-order loss was used to represent the complex process of chemical transformation of the solute.

Using the formulation of Cameron and Klute[4] and adding a first-order loss term,[16] the equation governing the transport of a chemically reactive solute is:

$$\frac{\partial}{\partial x_i}\left(D_{ij}\frac{\partial c}{\partial x_j}\right) - q_i\frac{\partial c}{\partial x_i} = \theta\frac{\partial c}{\partial t} + \frac{\partial(\rho_b c^*)}{\partial t} + f k_2 \rho_b c_k^* + q_s(c - c_s) \qquad \text{in } \Omega \tag{2a}$$

with

$$\frac{\partial(\rho_b c^*)}{\partial t} = k_1\theta c - k_2\rho_b c_k^* + \frac{\partial(\rho_b c_e^*)}{\partial t} \tag{2b}$$

where c is the solute concentration in the liquid (in units of mass per unit volume); c^* is the adsorbed phase concentration (in units of mass of adsorbed chemical per unit mass of porous media); c_k^* is the kinetic fraction of the adsorbed chemical and $c_e^*(= k_3\theta c/\rho_b)$ is the equilibrium fraction; k_1 is the forward (adsorption) rate constant, k_2 is the backward (desorption) rate constant and k_3 is the equilibrium constant; f is the loss coefficient for the selective first-order removal; q_i are the specific discharge components; ρ_b is the bulk density; q_s is the injected/pumped fluid volume per unit aquifer volume; and c_s is the solute concentration in q_s. D_{ij} is the hydrodynamic dispersion tensor computed on the basis of the specific discharge and is given by:

$$D_{ij} = (\alpha_L - \alpha_T)\frac{q_i q_j}{q} + \alpha_T q\,\delta_{ij} \tag{2c}$$

in which α_L is the longitudinal dispersivity; α_T is the transverse dispersivity; $q(= \sqrt{q_i q_i})$ is the magnitude of the specific discharge and δ_{ij} is the Kronecker delta ($\delta_{ij} = 1$ if $i = j$ and 0 otherwise).

As mentioned earlier, this model is equivalent to the mobile–immobile physical partitioning model

$$\frac{\partial}{\partial x_i}\left(D_{ij}\frac{\partial C_m}{\partial x_j}\right) - q_i\frac{\partial C_m}{\partial x_i} = (\theta_m + \rho_b f^* k)\frac{\partial C_m}{\partial t} + (\theta_{im} + (1 - f^*)\rho_b k)\frac{\partial C_{im}}{\partial t} \tag{3a}$$

with

$$(\theta_{im} + (1 - f^*)\rho_b k)\frac{\partial C_{im}}{\partial t} = \alpha_r(C_m - C_{im}) \tag{3b}$$

if we relate the parameters of these two models as:

$$c_k^* = \frac{\theta_{im} R_{im} C_{im}}{\rho_b}; \quad k_1 = \frac{\alpha_r}{\theta_m}; \quad k_2(1 - f) = \frac{\alpha_r}{R_{im}\theta_{im}}; \quad k_3 = \frac{f^* k \rho_b}{\theta_m} \tag{4}$$

in which θ_m and θ_{im} are the mobile and immobile phase water contents; C_m and C_{im} are the mobile and immobile zone solute concentrations; f^* is the fraction of solid matrix in contact with the mobile zone; k is the distribution coefficient; α_r is first-order rate constant; and $R_{im}(= 1 + \rho_b(1 - f^*)k/\theta_{im})$ is the retardation factor corresponding to the immobile zone. The similarity between the two models is made use of to compare the results of the numerical model with those obtained from an analytic solution of three-dimensional mobile–immobile partitioning model.

NUMERICAL SCHEME

Equation (1) is solved using the Galerkin technique by representing the pressure at any point (x_1, x_2, x_3) in the domain at any instant t as:

$$\psi(x_1, x_2, x_3, t) = N_I(x_1, x_2, x_3,)\psi^I(t) \tag{5}$$

where N_I are the shape functions associated with node I and ψ^I is the value of ψ at node I with the range of I being from 1 to NN (NN is the total number of nodes). Linear shape functions for triangular prism elements and tri-linear shape functions for the rectangular prism elements are used in this study. In a similar way, the hydraulic conductivity tensor and the moisture capacity term are represented as:

$$[K] = N_I[K]^I \tag{6a}$$

and

$$C = N_I C^I \tag{6b}$$

where $[K]$ and C are the conductivity tensor and the moisture capacity at any point in the domain at any time and $[K]^I$ and C^I are the nodal values. Strictly speaking, eqns (6a) and (6b) are inconsistent with eqn (5) because of the nonlinear relations between the pressure head and the unsaturated hydraulic conductivity, and relations between the pressure head and the moisture capacity term. Errors due to this inconsistent approach may however be resolved by using small elements. After these values of ψ, K and C are put in eqn (1), a residual R_ψ is obtained as:

$$R_\psi = \frac{\partial}{\partial x_i}\left((N_L K_{ij}^L)\frac{\partial}{\partial x_j}((N_J\psi^J) + x_3)\right) - ((N_L C^L) + \beta_s S_s)\frac{\partial}{\partial t}(N_J\psi^J) - q_s \tag{7}$$

Now using the Galerkin scheme, NN equations are

obtained as follows:

$$\int_\Omega R_\psi N_I \mathrm{d}\Omega = 0 \qquad \text{for } I = 1 \text{ to } NN \tag{8}$$

These equations can be more conveniently and concisely written in the matrix form, after making use of the divergence theorem and noting that the shape function for any node is nonzero only in elements containing that node, as:

$$[A]\{\psi\} + [B]\frac{\partial}{\partial t}\{\psi\} + \{F\} - \{Q\} = 0 \tag{9}$$

where $\{\psi\}$ is the vector of the nodal values of the pressure head; $[A]$ is the conductance matrix; $[B]$ is the storage matrix; $\{F\}$ is the gravity vector; and $\{Q\}$ is the flux vector. These matrices and vectors are given by the following equations:

$$\mathbf{A}_{IJ} = \sum_e \int_{V^e} \frac{\partial N_I}{\partial x_i}\left((N_L K_{ij}^L)\frac{\partial N_J}{\partial x_j}\right)\mathrm{d}V \tag{10a}$$

$$\mathbf{B}_{IJ} = \sum_e \int_{V^e} ((N_L C^L) + \beta_s S_s) N_I N_J \,\mathrm{d}V \tag{10b}$$

$$\mathbf{F}_I = \sum_e \int_{V^e} \frac{\partial N_I}{\partial x_i}(N_L K_{i3}^L)\,\mathrm{d}V \tag{10c}$$

$$\mathbf{Q}_I = \sum_e \left(\int_{V^e} -N_I q_s \,\mathrm{d}V + \int_{A^e} N_I q_b \,\mathrm{d}A \right) \tag{10d}$$

in which the integral is performed over all elements containing node I as one of their nodes and the boundary integral in eqn (10d) is evaluated along the boundaries of such elements which lie along the boundary of the domain with specified normal flux q_b. V_e represents the volume of the element and A_e its surface area. Equation (9) is solved by using a time-weighting scheme which results in the following equation:

$$\left(\xi[A] + \frac{[B]}{\Delta t}\right)\{\psi\}^{k+1} = \left(-(1-\xi)[A] + \frac{[B]}{\Delta t}\right)\{\psi\}^k + \{F\} - \{Q\} \tag{11}$$

in which the superscript denotes the time level and ξ is the time-weighting factor.

The set of algebraic equations are, then, solved using the pre-conditioned conjugate gradient method.[20,31] The incomplete LU (Lower and Upper triangular) decomposition of the coefficient matrix is used as a preconditioner to enhance the convergence properties of the method. Even with zero level of fill-in during the decomposition process, the convergence of conjugate gradient iteration was found to be adequate. Details of the procedure are given in Yeh and Srivastava.[30] Only the nonzero matrix elements need to be stored, thus saving a huge amount of computer memory as compared to the direct banded matrix solvers, more so in the three-dimensional case. The Picard iteration scheme is used to accomplish the convergence of the solution of the nonlinear algebraic equations. Automatic time stepping is used to ensure the convergence of the nonlinear iterations required because of the dependence of the coefficient matrices on the pressure head. The convergence of iterations is checked by comparing the maximum head difference between two successive iterations with a pre-specified tolerance. If the number of iterations exceeds a specified maximum or if the solution is found to be diverging, the time step is reduced by a specified factor. On the other hand, if the convergence is very rapid, the time step is automatically increased.

To avoid the loss of one order of accuracy due to the numerical differentiation in approximating the specific discharge field, a finite element type procedure[22,28] was employed, in which the velocities are obtained from the computed head field by applying the Galerkin technique separately to the flux equation:

$$q_i = -K_{ij}\frac{\partial}{\partial x_j}(\psi + x_3) \tag{12}$$

Using the same shape functions, N_I, for the velocity components, we obtain:

$$[A_q]\{q_i\} + [B_{qi}]\{\psi\} + \{C_{qi}\} = 0 \qquad \text{for } i = 1,2,3 \tag{13}$$

in which:

$$A_{q_{IJ}} = \sum_e \int_{v^e} N_I N_J \,\mathrm{d}V \tag{14a}$$

$$B_{qi_{IJ}} = \sum_e \int_{v^e} N_I K_{ij}\frac{\partial N_J}{\partial x_j}\,\mathrm{d}V \tag{14b}$$

$$C_{qi_I} = \sum_e \int_{v^e} N_I K_{i3}\,\mathrm{d}V \tag{14c}$$

Although this procedure involves solution of NN simultaneous equations for each velocity component, the coefficient matrix is time invariant and has to be inverted only once during the entire simulation.

Equations (2) are solved using one-step reverse particle tracking for the advective transport (called MMOC for modified method of characteristics) and the regular Galerkin FEM for the dispersive transport. In the MMOC, the partial time derivative in eqn (2a) is converted to a total derivative along the characteristic lines by using:

$$\frac{\mathrm{D}c}{\mathrm{D}t} = \frac{\partial c}{\partial t} + \frac{q_i}{\theta(1+k_3)}\frac{\partial c}{\partial x_i} \tag{15}$$

The finite difference form of the time derivative can be written as

$$\frac{\mathrm{D}c}{\mathrm{D}t} = \frac{c^{k+1} - c_n^k}{\Delta t}$$

in which c_n^k is the concentration at the time level k at the corresponding spatial position along the characteristic

line. After applying the Galerkin technique to the dispersive part of the equation, the concentration at a time step is given by:

$$\left(\xi[A_c] + \left(\frac{\xi k_1}{1 + k_2 \xi \Delta t} + \frac{1 + k_3}{\Delta t}\right)[B_c]\right)\{c^{k+1}\} = \left(-(1-\xi)[A_c] - \frac{(1-\xi)k_1}{1 + k_2 \xi \Delta t}[B_c]\right)\{c^k\} + \frac{1 + k_3}{\Delta t} \times [B_c]\{c_n^k\} + \frac{[B_c^*]}{1 + k_2 \xi \Delta t}\{c_k^{*k}\} - \{Q_c\} \tag{16}$$

in which:

$$A_{c_{IJ}} = \sum_e \int_{v^e} D_{ij} \frac{\partial N_I}{\partial x_i} \frac{\partial N_J}{\partial x_j} \mathrm{d}V \tag{17a}$$

$$B_{c_{IJ}} = \sum_e \int_{v^e} \theta N_I N_J \, \mathrm{d}V \tag{17b}$$

$$B^*_{c_{IJ}} = \sum_e \int_{V^e} \rho_b k_2 N_I N_J \, \mathrm{d}V \tag{17c}$$

$$Q_{c_I} = \sum_e \left(\int_{V^e} N_I q_s (c - c_s) \, \mathrm{d}V - \int_{A^e} N_I q_{cb} \, \mathrm{d}A \right) \tag{17d}$$

The boundary integral in eqn (17d) is performed over boundaries with specified dispersive flux q_{cb}.

The location for the determination of c_n^k is obtained by fourth-order Runge–Kutta integration of the equation:

$$\frac{\mathrm{d}x_i}{\mathrm{d}t} = \frac{q_i}{\theta(1 + k_3)} \tag{18}$$

resulting in the following expressions:

$$\mathrm{d}x_i^1 = -\frac{\Delta t (q_i^{k+1})_{x_i}}{\theta_{x_i}^{k+1}(1 + k_3)} \tag{19a}$$

$$\mathrm{d}x_i^2 = -\frac{\Delta t (q_i^{k+1} + q_i^k)_{x_i + (\mathrm{d}x_i^1/2)}}{(\theta^{k+1} + \theta^k)_{x_i + (\mathrm{d}x_i^1/2)}(1 + k_3)} \tag{19b}$$

$$\mathrm{d}x_i^3 = -\frac{\Delta t (q_i^{k+1} + q_i^k)_{x_i + (\mathrm{d}x_i^2/2)}}{(\theta^{k+1} + \theta^k)_{x_i + (\mathrm{d}x_i^2/2)}(1 + k_3)} \tag{19c}$$

$$\mathrm{d}x_i^4 = -\frac{\Delta t (q_i^k)_{x_i + \mathrm{d}x_i^3}}{\theta^k_{x_i + \mathrm{d}x_i^3}(1 + k_3)} \tag{19d}$$

and

$$x_i^k = x_i + \tfrac{1}{6}(\mathrm{d}x_i^1 + 2\mathrm{d}x_i^2 + 2\mathrm{d}x_i^3 + \mathrm{d}x_i^4) \tag{19e}$$

During the back-tracking algorithm, if the particle crosses an inflow boundary, it is assigned the concentration at the boundary. At no flow boundaries, the particle is reflected back into the domain. After solving for the liquid phase concentration from eqn (16), the adsorbed phase concentration is obtained from:

$$c_k^{*k+1} = \frac{(1 - k_2(1-\xi)\Delta t)c_k^{*k} + \frac{(1-\xi)k_1\theta\Delta t}{\rho_b}c^k + \frac{\xi k_1 \theta \Delta t}{\rho_b}c^{k+1}}{1 + k_2 \xi \Delta t} \tag{20a}$$

and

$$c_e^{*k+1} = k_3 \frac{\theta}{\rho_b} c^{k+1} \tag{20b}$$

If the time weighting factor ξ is taken to be 0, we obtain an explicit scheme which, along with the lumping of the mass matrix, results in direct evaluation of nodal concentration at time level $(k + 1)$ without solving a set of linear simultaneous equations. This results in considerable saving of computer time and storage space. A value of ξ less than 0·5, however, restricts the time-step size to ensure stability of the numerical scheme. In case of MMOC, though, comparatively larger time steps can be used without producing instability because the convective part of the transport is handled by reverse particle tracking. The disadvantage of using large time-step size is decreased accuracy of results because of the time discretization. On the other hand, it also implies less accumulation of error due to interpolation of concentration values during back-tracking because the number of time steps will be smaller. The relative magnitude of these two counteracting processes will be largely problem dependent. Comparison of results from the explicit and implicit schemes indicates a saving of about 25% in the CPU time for the explicit method for large problems involving tens of thousands of nodes and up to 60% saving for smaller problems.

After solving for the head in the flow part and the concentration in the transport part, a mass balance check for both water and solute is performed. Almost in all applications described in the next section, the mass balance was quite satisfactory and the error was mostly less than 1% for water flow and 5% for solute transport.

APPLICATIONS

The model is first applied to the transport of a reactive chemical in one-dimensional saturated flow for which analytic solution is given by Cameron and Klute.[4] Breakthrough curves obtained from the numerical model are compared with experimental observations. The next application involves two-dimensional unsaturated flow and transport towards the water table. Analytic solution to the flow part of the problem is derived (see Appendix), if an exponential relationship is assumed between the pressure and conductivity and between pressure and moisture content. Finally, the

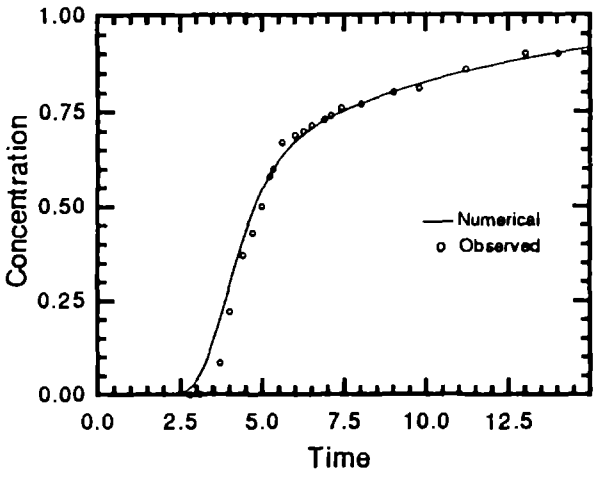

Fig. 1. Comparison of numerical solution with observed breakthrough curve for Atrazine.

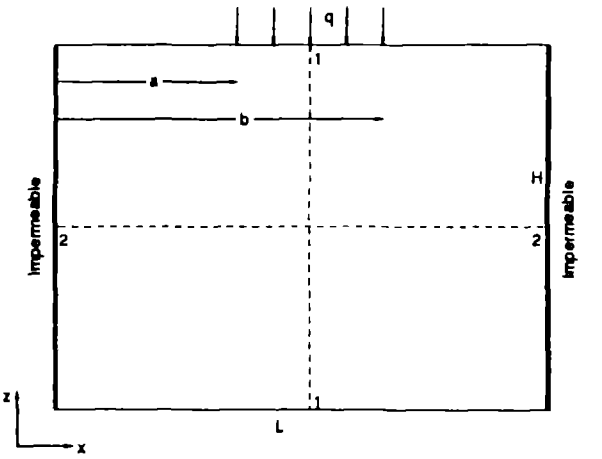

Fig. 2. Schematic diagram for two-dimensional unsaturated flow and transport.

model is applied to simulate a three-dimensional transport situation for which analytic solution is available for various types of solute input conditions if we use the physical partitioning model.[11]

1D saturated flow and transport

The numerical scheme described above is first used to simulate the transport of Atrazine in a Honeywood silt loam soil column under a saturated condition. Breakthrough data were collected by Elrick *et al.*[9] Cameron and Klute[4] present an analytic solution to this problem assuming a semi-infinite medium with concentration type boundary condition at the upstream end and zero concentration at infinity. Nondimensional parameters are defined as:

$$T = \frac{vt}{L}; \qquad B = \frac{vL}{4D}; \qquad C = \frac{c}{c_0}$$

$$K_1 = \frac{Lk_1}{v}; \qquad K_2 = \frac{Lk_2}{v}; \qquad K_3 = k_3$$

where t is time; L is the length of the medium; v is the seepage velocity; D is the hydraulic dispersion coefficient; c_0 is the specified concentration at the upstream end and B is the Brenner number.

For the numerical simulation, B is taken as 10 and the breakthrough curve (plots of dimensionless time versus dimensionless exit concentration) for the chemical Atrazine, with $K_1 = 0{\cdot}48$, $K_2 = 0{\cdot}18$ and $K_3 = 3{\cdot}52$, is shown in Fig. 1. The mesh Peclet number is kept at 0·4 and the Courant number is equal to 1. The time-weighting factor in this simulation is 0·5, resulting in the time-centered (Crank–Nicholson) scheme. It is seen that the MMOC duplicates the observed breakthrough data very well, though it should be mentioned that the reaction parameters were obtained by fitting the analytic solution to the observed data.[4] Also, taking the Courant number equal to 1 results in nodes being tracked to nodes, thus eliminating the interpolation error. Additional runs with Courant number equal to 2 and 0·5 gave almost identical results, indicating that the interpolation errors do not play a major role in this problem.

2D flow and transport in variably saturated media

The second application of the model is to the case of solute transport in a hypothetical soil profile under steady flow toward the water table from a strip source. Steady-state flow and velocity fields were simulated first and a constant concentration boundary condition was then imposed on the strip source to simulate the transport of solute under the unsaturated condition. Exponential relations are assumed between the pressure and conductivity and pressure and moisture content relationships of the hypothetical soil. Figure 2 shows the schematic of the solution domain and the boundary conditions. Initial conditions are assumed to be hydrostatic and the parameters used are:

$$K_{sx} = K_{sz} = 1\,\text{cm/h}; \quad \alpha = 0{\cdot}01/\text{cm} \quad \theta_s = 0{\cdot}44;$$

$$\theta_r = 0{\cdot}067; \quad \alpha_L = \alpha_T = 1{\cdot}0\,\text{cm}; \quad L = 15\,\text{cm};$$

$$H = 10\,\text{cm}; \quad a = 6\,\text{cm}; \quad b = 9\,\text{cm}; \quad q = 0{\cdot}5\,\text{cm/h}$$

where K_{si} is the saturated conductivity in the i-direction; α is pore-size distribution parameter; θ_s is the saturated water content; and θ_r is the residual water content.

The domain was divided into 2500 elements with 5202 nodes for the 3D model (one element wide in the y-direction) with $\Delta x = 0{\cdot}3\,\text{cm}$, $\Delta y = 1{\cdot}0\,\text{cm}$ and $\Delta z = 0{\cdot}2\,\text{cm}$. To check the accuracy of the numerical solution, analytical solutions for the velocity components in x- and z-directions were derived and are listed in the Appendix. Figures 3(a) and (b) show the profiles of vertical velocity components obtained from the numerical model at sections 1–1 and 2–2 respect-

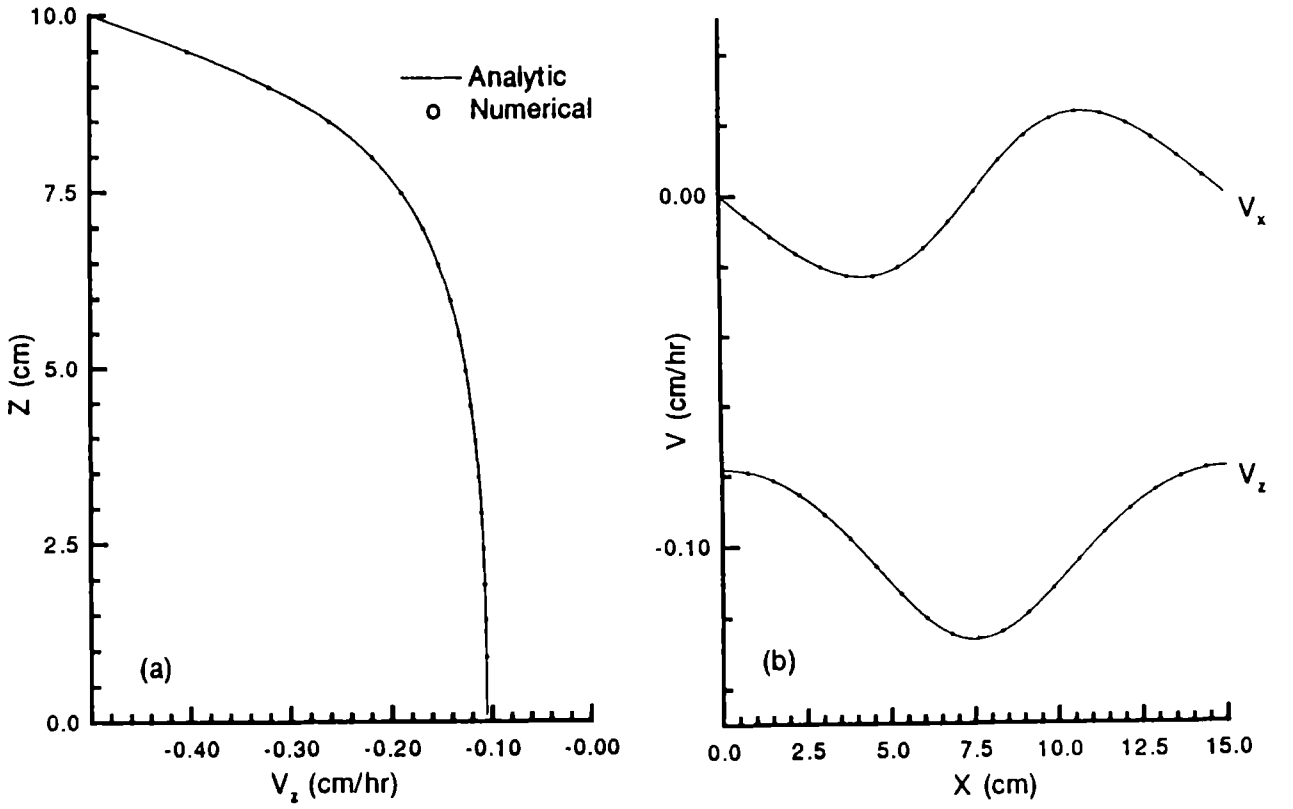

Fig. 3. Comparison of velocity profiles along (a) section 1–1 and (b) section 2–2.

ively (see Fig. 2). Also shown are the analytic results from the steady-state solution, and clearly the numerical results are in excellent agreement with the analytic solutions. This indicates that, for this problem, the inconsistency of assuming both the heads and the velocity components as linear does not adversely affect the results. It was, however, observed that the velocity components at the inflow boundary obtained from the numerical solution were slightly different from the specified values. Also, a very small velocity component was obtained at the no-flow boundaries. This was thought to be a result of discretization error and was handled by forcing the components at the boundaries to be equal to the specified values prior to the solution of the set of equations.

Simulated solute distributions at various times are depicted in Fig. 4. The simulated distributions appear reasonable. However, in the absence of analytic solutions for solute transport for the specified flow field, we cannot verify the accuracy of the results. A check of mass balance shows that MMOC has quite good mass balance properties. The mass balance error, as mentioned earlier, was less than 5%. To test the model against high Peclet numbers, the same problem was solved with zero dispersivity ($\alpha_L = \alpha_T = 0$) and the corresponding results are shown in Fig. 5. The sharpness of the solute profile as compared to the previous figure is evident from these figures.

3D flow and transport in saturated media

The final application of the model is to the transport of a solute pulse introduced in a rectangular prism portion of a three-dimensional porous medium (Fig. 6). The flow is assumed to be uni-directional and the medium is fully saturated. An analytic solution to this problem for infinite medium and with mobile–immobile physical partitioning model is available (Goltz and Roberts;[11] their equations (4) and (16)). The parameter values for the first simulation were taken as those given in Goltz and Roberts[11] (their Fig. 3), with slight modification:

$$\theta_m = 0{\cdot}342;\ \theta_{im} = 0{\cdot}038;\ R_m = 2{\cdot}78;\ R_{im} = 5{\cdot}00;$$

$$v_m = 0{\cdot}091\ \text{m/day};\ D_{mx} = 0{\cdot}02\ \text{m}^2/\text{day};\ D_{my} = D_{mz} = 0{\cdot}0016\ \text{m}^2/\text{day};\ \alpha_r = 0{\cdot}006/\text{day}$$

The half-width, length and depth of the solute pulse were taken as $L = 1$ m, $M = 0{\cdot}5$ m and $N = 0{\cdot}5$ m and the sampling point was located at $L = 3$ m, $m = 0$ and $n = 0$ m (from the center of the pulse). The equivalent parameters for the chemical transport model are:

$$k_1 = 0{\cdot}0175/\text{day};\quad (1-f)k_2 = 0{\cdot}0316/\text{day};$$

$$k_3 = 1{\cdot}78$$

Also, the longitudinal dispersivity was taken as 0·2198 m and the transverse dispersivity as 0·0176 m. The specific

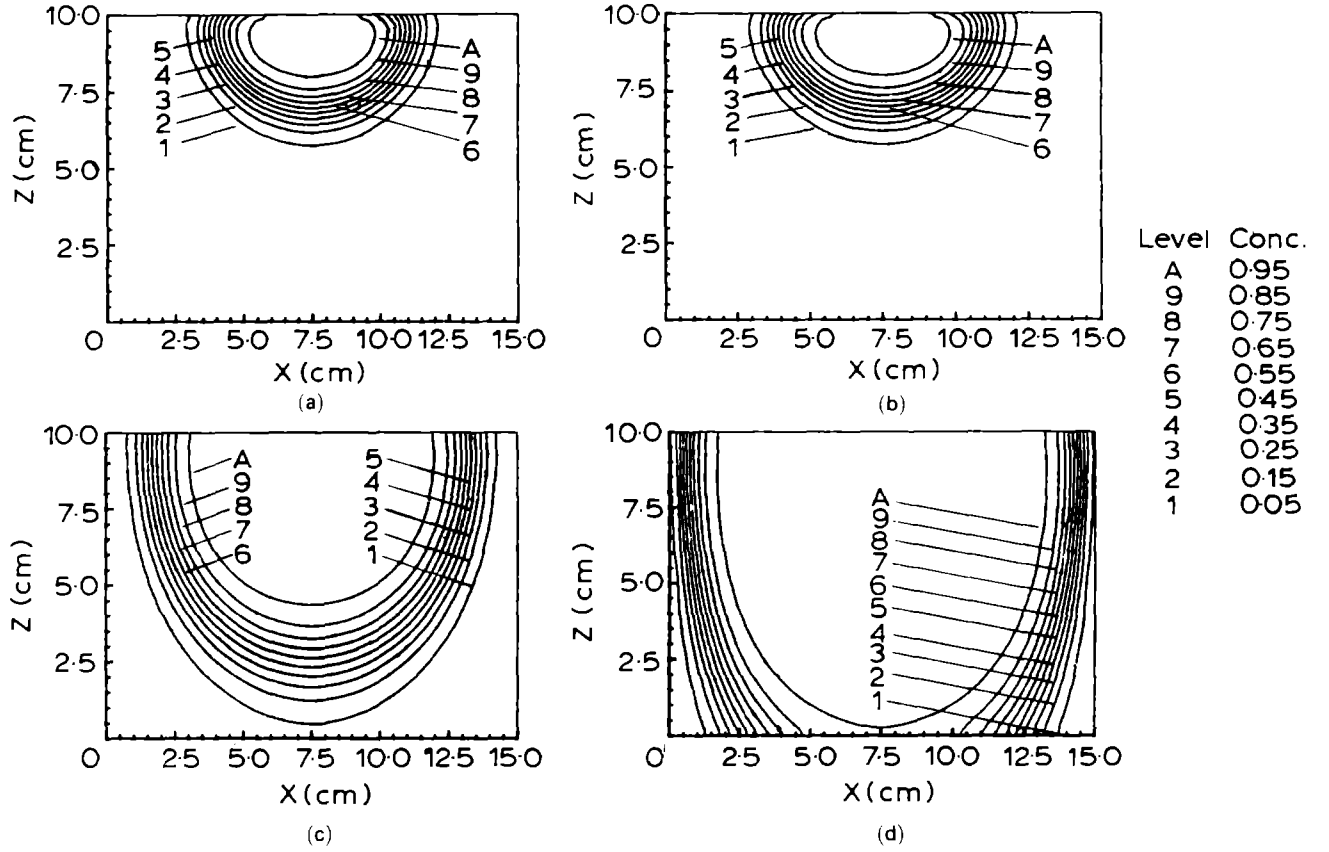

Fig. 4. Concentration contours at various times: (a) 5 h, (b) 10 h, (c) 20 h, and (d) 40 h.

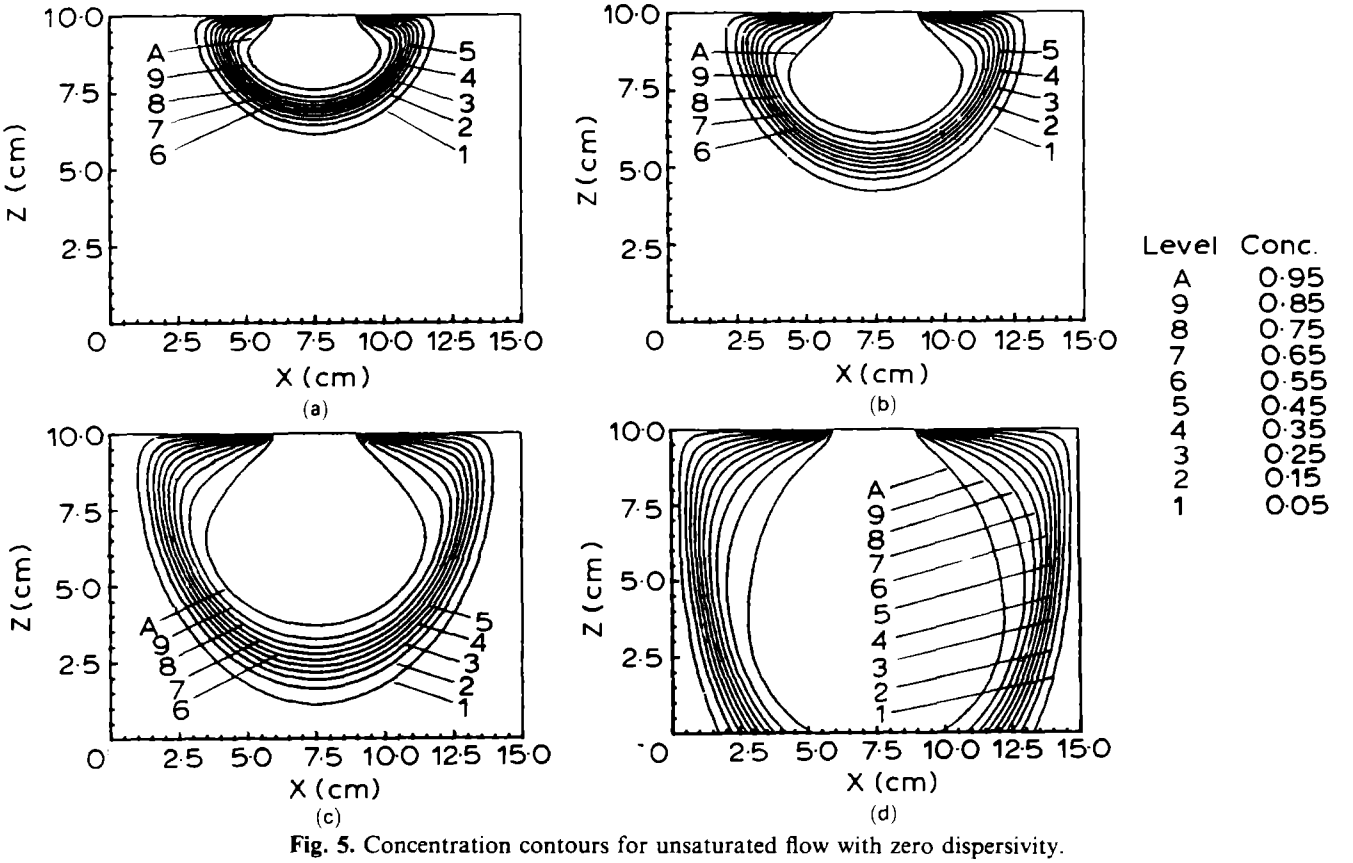

Fig. 5. Concentration contours for unsaturated flow with zero dispersivity.

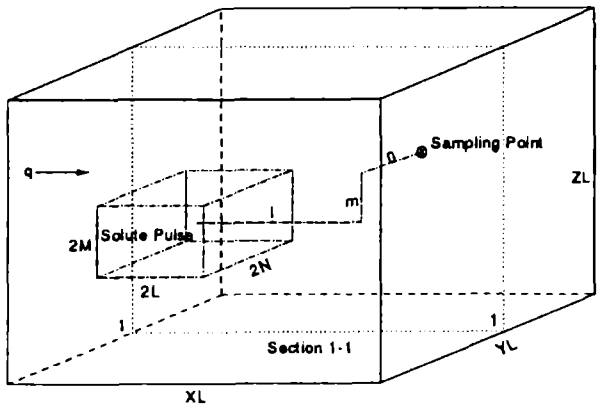

Fig. 6. Schematic diagram for three-dimensional flow and transport.

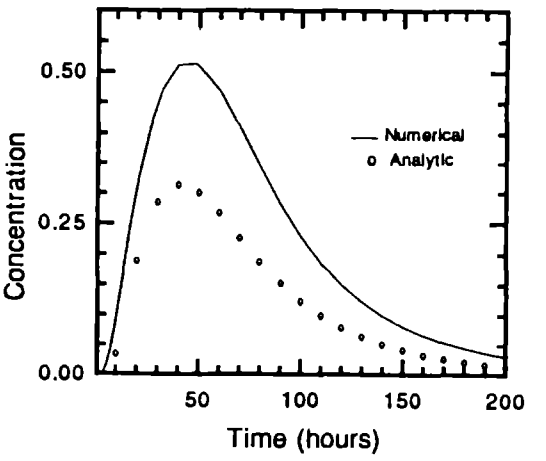

Fig. 7. Breakthrough curve at the sampling point with the solute pulse coinciding with the finite element grid.

discharge q_x is 0·0311 m/day. The domain modeled was chosen to be 20 m × 2 m × 2 m, which was divided into 6400 elements with 8181 nodes with $\Delta x = 0{\cdot}2$ m, $\Delta y = 0{\cdot}25$ m and $\Delta z = 0{\cdot}25$ m.

Figure 7 shows the breakthrough curve at the sampling point computed from the analytic solution and also from the numerical method using the MMOC. Although a fair matching of the time of arrival of the peak is observed, the numerical solution is considerably higher than the analytic one. A similar trend was observed in the concentration contours along section 1–1, a sample of which, at 200 days after the introduction of the pulse, is shown in Fig. 8. The main reason for this difference was thought to be stemming from the initial distribution of solute in the numerical scheme. The finite element grid is constructed in such a way that the rectangular prism of the solute pulse coincides with the discretizing nodes. As a result, the

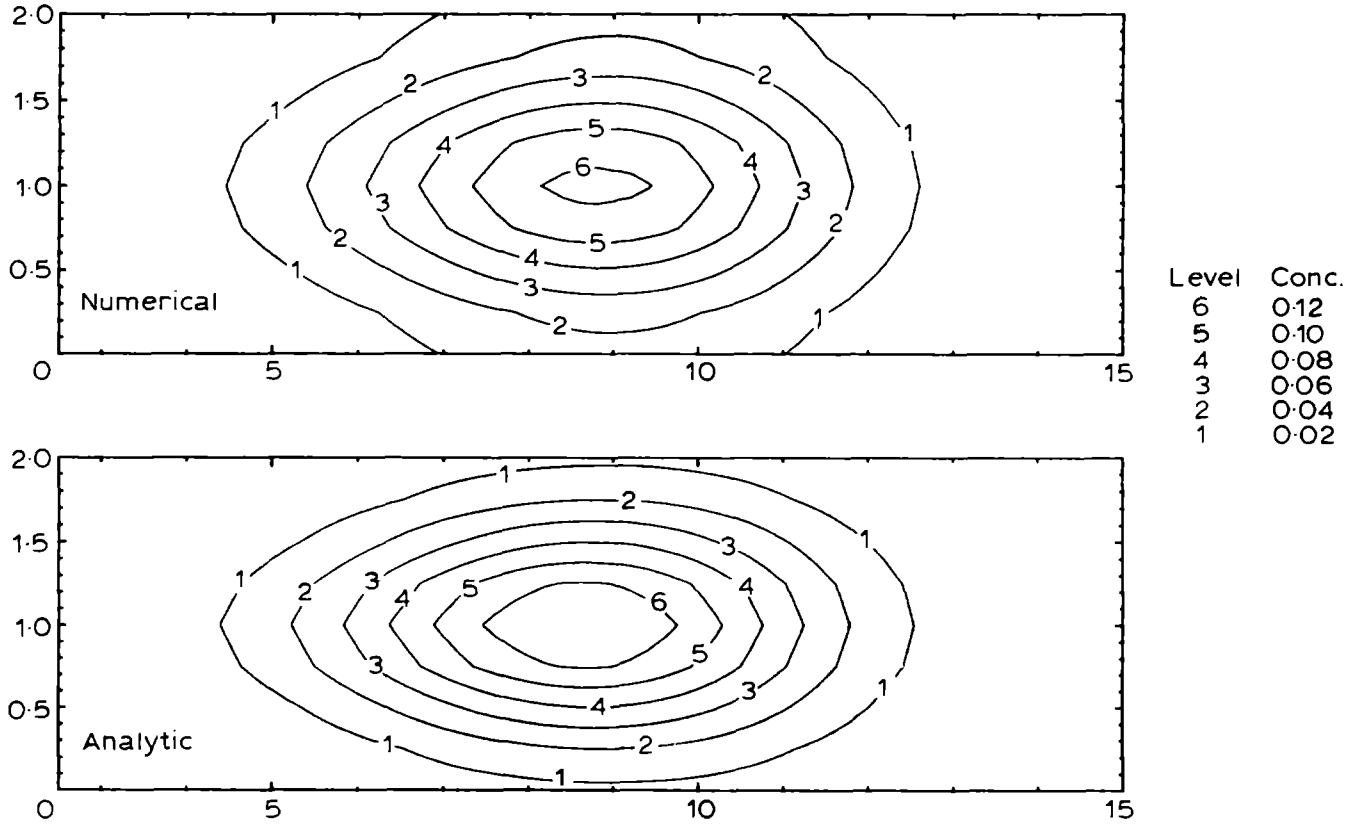

Fig. 8. Concentration contours along section 1–1 at 200 h.

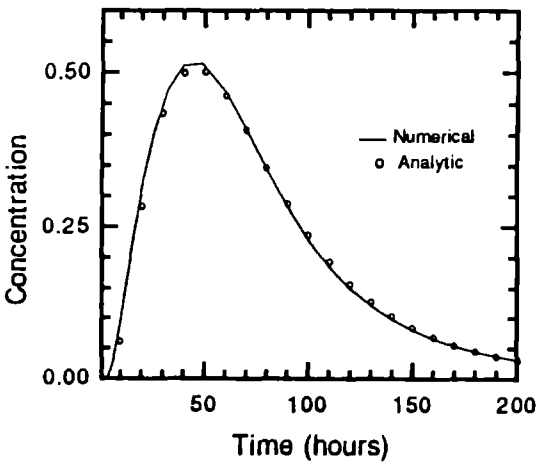

Fig. 9. Breakthrough curve at the sampling point with the solute pulse centered within an element.

initial concentration at those nodes is specified as unity while the nodes adjacent to them have zero concentration. And since a linear shape function is used, the numerical scheme assumes a linear variation from one to zero in the elements adjacent to the pulse. Thus, we have extra mass in the system, which manifests itself in higher concentration values in the numerical simulation.[25] To test this hypothesis, later simulations were done with finite element grid constructed in such a way as to put the pulse halfway in an element. The numerical results are found to be in much better agreement with the analytic solution as shown in the next figures (Figs 9 and 10). For these figures the analytic solution is obtained by increasing the dimension of the initial solute prism to 2·2 m × 0·75 m × 0·75 m. Very good initial matching was observed but the numerical solution again has a tendency to get larger than the analytic solution with the passage of time (Fig. 10). This can be explained by the fact that the analytic solution assumes an infinite domain, while the numerical solution is for a finite domain. This results in solute being reflected by the domain boundaries and increasing the concentration in the numerical solution. At early times, the plume has not spread to an extent where it is affected by the boundary and therefore excellent agreement between the two solutions was seen. Figure 10 is a very clear demonstration of the effect of the boundaries. Figures 11 and 12 show the same type of profiles but with a ten-fold reduction in the dispersivity values (and a corresponding increase in the Peclet number). Again, the movement of the center of mass is well duplicated, but numerical dispersion is apparent from the contours. The lower dispersivity reduces the boundary effect because of less spreading and reasonable match near the top and bottom boundaries is observed. Along the flow direction, however, a little numerical dispersion can be noticed.

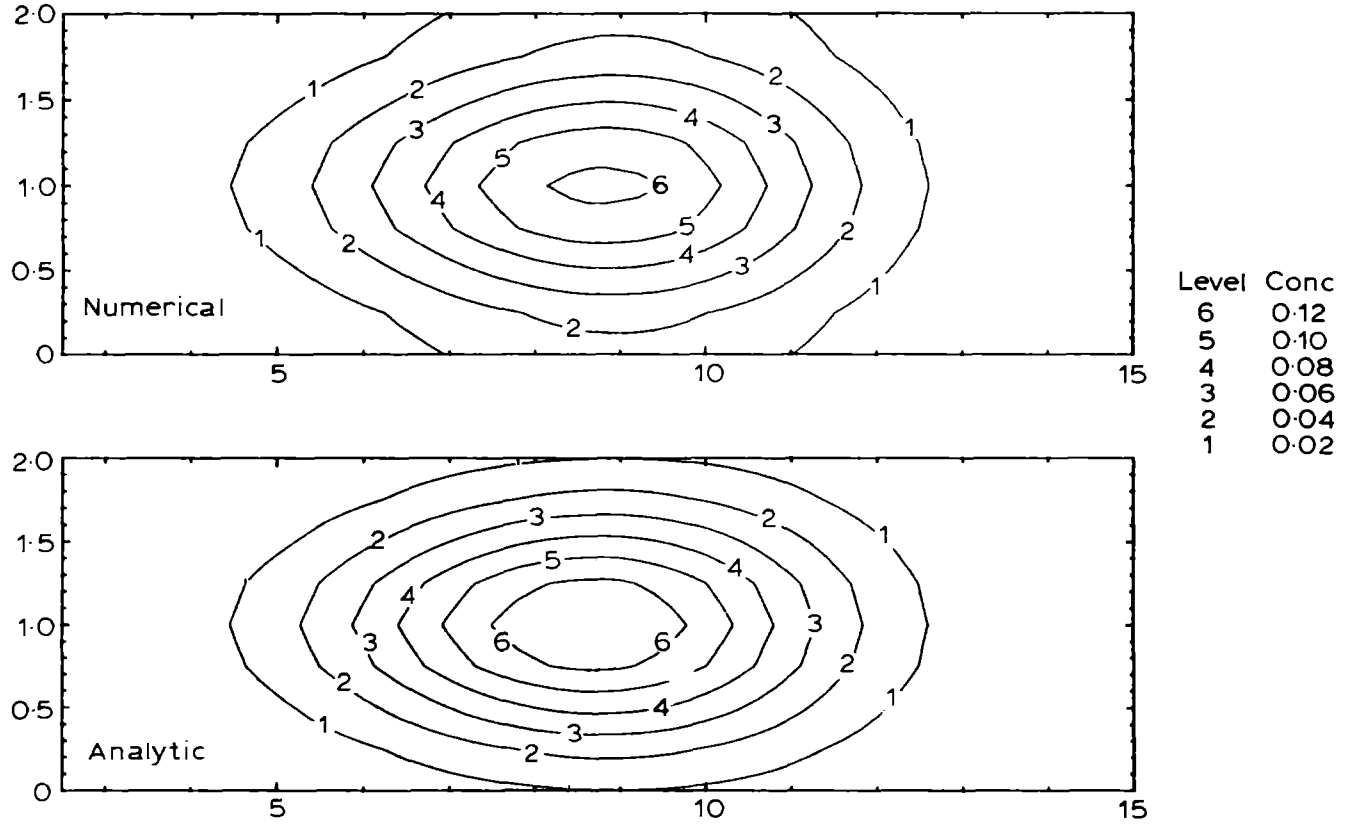

Fig. 10. Concentration contours along section 1–1 at 200 h.

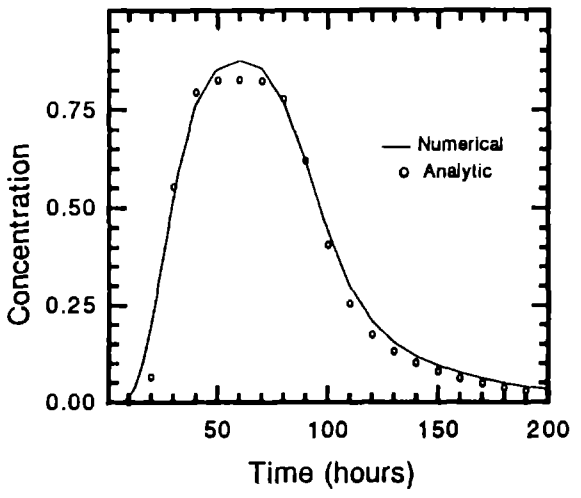

Fig. 11. Breakthrough curve at the sampling point for the low dispersivity case.

SUMMARY

A three-dimensional finite element model for the simulation of the transport of a chemically reactive solute is developed by combining the recent developments in the fields of numerical methods and chemical reaction of solvents. The accuracy of this model is verified against analytic solutions and observed values for both saturated and unsaturated flow and transport problems. Some observations based upon various runs with the authors' model are summarized below. (i) Always use the automatic time-stepping and lumped scheme options. Based on experiences, large element sizes and small time steps will speed up the convergence at each time step. This is due to the fact that the coefficient matrix becomes diagonally dominant and radius of convergence is greatly expanded.[10] However, the trade-off is that it will take a large number of time steps to finish the simulation resulting in a possible increase in interpolation error during reverse particle tracking. (ii) A fully explicit scheme can be used in conjunction with the MMOC to save computer time and storage space without limiting the time step to a very small value. (iii) In most flow situations the application of Galerkin scheme to the flux equation results in quite accurate velocity field although assumption of linear variation of velocity is inconsistent with a linear head variation. Near the boundaries, however, this approach fails to simulate accurately the velocity components. Currently, the model is being applied to simulate migration of chloride and colloids in a large-scale field experiment and the preliminary results appear to be quite encouraging.

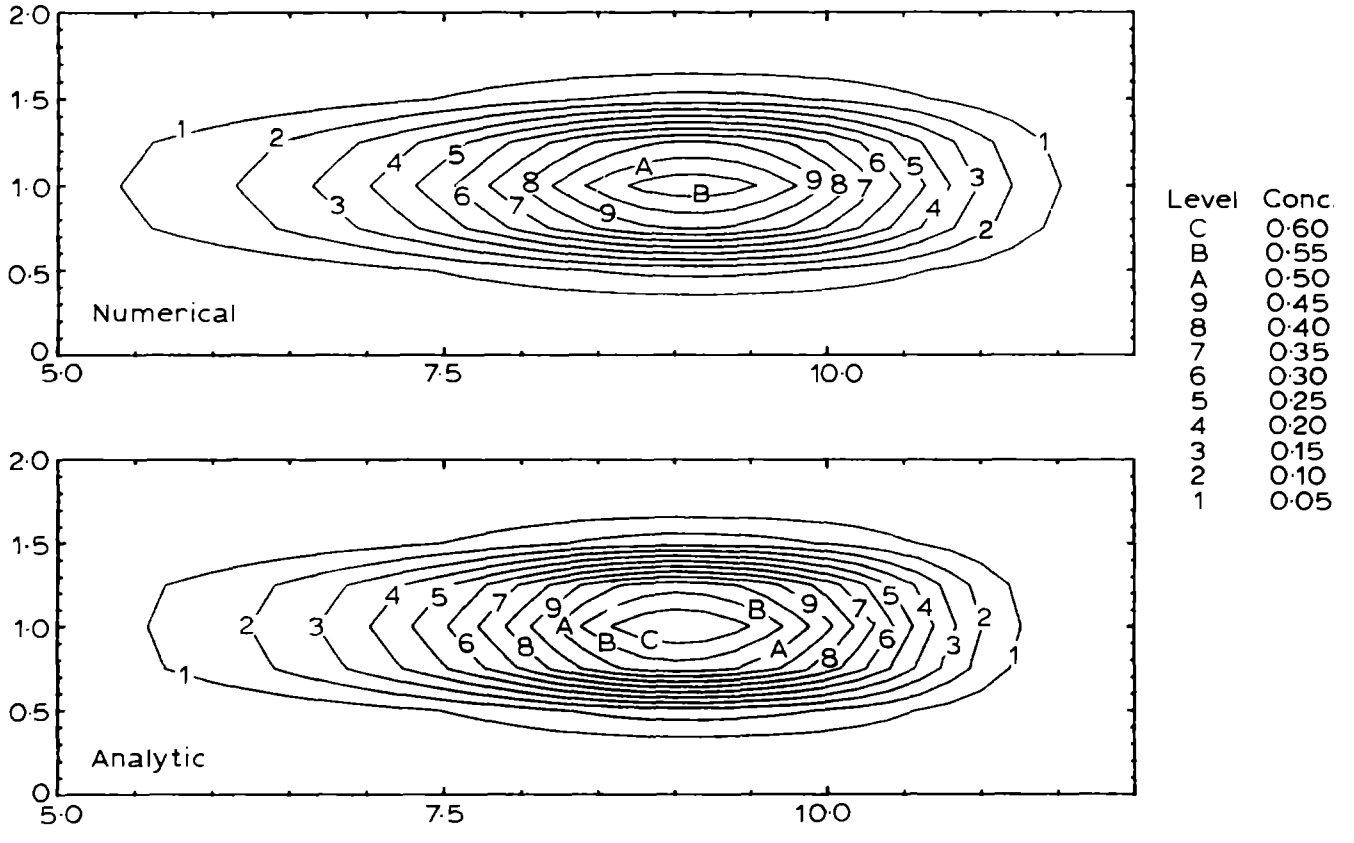

Fig. 12. Concentration contours along section 1–1 at 200 h for low dispersivity case.

ACKNOWLEDGMENTS

The authors wish to thank the anonymous reviewers for their valuable suggestions, which resulted in improved presentation of this article. This study is funded in part by EPA grant R-813899-01-1 and in part by DOE grant DE-FG02-91-ER61199 from the office of basic energy sciences.

REFERENCES

1. Anderson, M.P., Using models to simulate the movement of contaminants through ground water flow systems. *CRC Crit. Rev. Environ. Control*, **9** (1979) 97–156.
2. Bear, J., *Hydraulics of Groundwater*. McGraw Hill, New York, 1979.
3. Cady, R., An adaptive multi-dimensional finite element method for simulating advectivion–dispersion. PhD dissertation, Dept. of Hydrology and Water Resources, University of Arizona, Tucson, AZ, 1991.
4. Cameron, D.R. & Klute, A., Convective–dispersive solute transport with a combined equilibrium and kinetic model. *Water Resour. Res.*, **13** (1977) 183–8.
5. Celia, M.A., Bouloutas, E.T. & Zarba, R.L., A general mass-conservative numerical solution for the unsaturated flow equation. *Water Resour. Res.*, **26** (1990) 1483–96.
6. Chiang, C.Y., Wheeler, M.F. & Bedient, P.B., A modified method of characteristics technique and mixed finite elements method for simulation of ground water solute transport. *Water Resour. Res.*, **25** (1989) 1541–9.
7. Coats, K.H. & Smith, B.D., Dead end pore volume and dispersion in porous media. *Soc. Pet. Eng. J.*, **4** (1964) 73–84.
8. Deans, H.A., A mathematical model for dispersion in the direction of flow in porous media. *Soc. Pet. Eng. J.*, **3** (1963) 49–52.
9. Elrick, D.E., Erh, K.T. & Krupp, H.K., Application of miscible displacement techniques to soils. *Water Resour. Res.*, **2** (1966) 717–27.
10. Fletcher, C.A.J., *Computational Techniques for Fluid Dynamics. Springer Series in Computational Physics*. Springer-Verlag, New York, 1988.
11. Goltz, M.N. & Roberts, P.V., Three-dimensional solutions for solute transport in an infinite medium with mobile and immobile zones. *Water Resour. Res.*, **22** (1986) 1139–48.
12. Goode, D.J., Particle velocity interpolation in block-centered finite difference groundwater flow models. *Water Resour. Res.*, **26** (1990) 925–40.
13. Huyakorn, P.S. & Nilkuha, K., Solution of transient transport equation using an upstream finite element scheme. *Appl. Math. Model.*, **3** (1979) 7–17.
14. Konikow, L.F. & Bredehoeft, J.D., Computer model of two-dimensional solute transport and dispersion in ground water. In *Techniques of Water Resources Investigations, Book 7*. US Geol. Survey, Reston, VA, 1978, chap. 2.
15. Krupp, H.K., Biggar, J.W. & Nielsen, D.R., Relative flow rates of salt and water in soil. *Soil Sci. Soc. Am. J.*, **36**(3) (1972) 412–17.
16. Lassey, K.R., Unidimensional solute transport incorporating equilibrium and rate-limited isotherms with first order loss. 1. Model conceptualizations and analytic solutions. *Water Resour. Res.*, **24** (1988) 343–50.
17. Lindstrom, F.T. & Boersma, L., A theory on the mass transport of previously distributed chemicals in a water-saturated sorbing porous medium. III, Exact solutions for first order kinetic sorbtion. *Soil Sci.*, **115**(1) (1973) 5–10.
18. Neuman, S.P., Adaptive Eulerian–Lagrangian finite element method for advection–dispersion. *Int. J. Numer. Methods Engg*, **20** (1984) 321–37.
19. Nkedi-Kizza, P. *et al.*, On the equivalence of two conceptual models for describing ion-exchange during transport through an aggregated oxisol. *Water Resour. Res.*, **20** (1984) 1123–30.
20. Reid, J.K., On the method of conjugate gradients for the solution of large sparse systems of linear equations. In *Proc. Conf. on Large Sparse Sets of Linear Equations*, ed. J.K. Reid. Academic Press, New York, pp. 231–54.
21. Rubin, J., Transport of reactive solutes in porous media: Relation between mathematical nature of problem formulation and chemical nature of reactions. *Water Resour. Res.*, **19** (1983) 1231–52.
22. Segol, G., A three-dimensional Galerkin finite element model for the analysis of contaminant transport in variably saturated–unsaturated porous media. Department of Earth Sciences, University of Waterloo, Waterloo, Canada, 1976.
23. Selim, H.M., Davidson, J.M. & Mansell, R.S., Evaluation of a two-site adsorption–desorption model for describing solute transport in soils. In *Proc. Summer Comp. Simul. Conf.* Simulations Councils, Inc., La Jolla, CA, 1976, pp. 444–8.
24. Sudicky, E.A., The Laplace transformation Galerkin technique: A time continuous finite element theory and application to mass transport in ground water. *Water Resour. Res.*, **25** (1989) 1833–46.
25. van Genuchten, M.Th., On the accuracy and efficiency of several numerical schemes for solving the convective–dispersive equation. In *Finite Elements in Water Resources*, ed. W.G. Gray, G.F. Pinder & C.A. Brebbia. Pentech Press, London, 1977, pp. 1.71–1.90.
26. van Genuchten, M.Th. & Wierenga, P.J., Mass transfer studies in sorbing porous media 1. Analytical solutions. *Soil Sci. Soc. Am. J.*, **40** (1976) 473–80.
27. Yanosik, J. & McCracken, T., A nine-point finite difference reservoir simulation for realistic prediction of adverse mobility ratio displacements. *Soc. Pet. Eng. J.*, **19** (1979) 253–62.
28. Yeh, G.T., On the computation of Darcian velocity and mass balance in the finite element modeling of groundwater flow. *Water Resour. Res.*, **17** (1981) 1529–34.
29. Yeh, G.T., A Lagrangian-Eulerian method with zoomable hidden fine-mesh approach to solving advection–dispersion equations. *Water Resour. Res.*, **26** (1990) 1133–44.
30. Yeh, T.-C.J. & Srivastava, R., Variably saturated flow and transport in 2 dimensions. Technical Report No. HWR 90-010, University of Arizona, Tucson, AZ, 1990.
31. Young, D.M., *Iterative Solution of Large Linear Systems*. Academic Press, New York, 1971.

APPENDIX

The analytic solution of two-dimensional steady-state flow towards water table is given below. The flow domain is of height H and length L and the recharging strip extends from a distance a to b from the left-hand-side. Both the vertical sides are impervious and the lower boundary is the water table. The flow through the strip is q. The origin of coordinates in the following

expressions is at the lower left corner of the domain. The actual variables are denoted with an asterisk to distinguish them from their dimensionless forms. Exponential relations are assumed as follows:

$$K_x^* = K_{sx}e^{\alpha\psi};\ K_z^* = K_{sz}e^{\alpha\psi};\ \theta = \theta_r + (\theta_s - \theta_r)e^{\alpha\psi} \quad \text{(A1)}$$

where K_i^* is the hydraulic conductivity in the i-direction.

Dimensionless variables are defined as:

$$x = \alpha x^* \sqrt{\frac{K_{sz}}{K_{sx}}} \text{ so that } L = \alpha L^* \sqrt{\frac{K_{sz}}{K_{sx}}};$$

$$a = \alpha a^* \sqrt{\frac{K_{sz}}{K_{sx}}};\ b = \alpha b^* \sqrt{\frac{K_{sz}}{K_{sx}}} \quad \text{(A2)}$$

$$z = \alpha z^* \text{ so that } H = \alpha H^* \quad \text{(A3)}$$

$$K = \frac{K_x^*}{K_{sx}} = \frac{K_z^*}{K_{sz}} \quad \text{(A4)}$$

$$q = \frac{q^*}{K_{sz}} \quad \text{(A5)}$$

The steady-state solution is given by:

$$K = e^{-z} + \frac{q(b-a)}{L}(1 - e^{-z}) + \frac{2q}{L}e^{H-z/2} \times \sum_{n=1}^{\infty} \frac{\{\sin(\lambda_n b) - \sin(\lambda_n a)\}\cos(\lambda_n x)\sinh(p_n z)}{\lambda_n\{\frac{1}{2}\sinh(p_n H) + p_n \cosh(p_n H)\}} \quad \text{(A6)}$$

where $\lambda_n = n\pi/L$ and $p_n = \sqrt{\frac{1}{4} + \lambda_n^2}$.

The dimensionless Darcy velocity components in the x- and z-directions are obtained as:

$$V_x = \frac{V_x^*}{\sqrt{K_{sx}K_{sz}}} = -\frac{\partial K}{\partial x} \quad \text{(A7)}$$

and

$$V_z = \frac{V_z^*}{K_{sz}} = -\left(\frac{\partial K}{\partial z} + K\right) \quad \text{(A8)}$$